

Semiconducting polymer waveguides for end-fired ultra-fast optical amplifiers

Ning Liu, Arvydas Ruseckas, Neil A. Montgomery, Ifor D. W. Samuel,
and Graham A. Turnbull*

*Organic Semiconductor Centre, SUPA, School of Physics and Astronomy, University of St Andrews,
North Haugh, St Andrews, Fife KY16 9SS, U.K.*

**gat@st-and.ac.uk*

Abstract: A method to fabricate conjugated polymer waveguides with well defined edge facets is demonstrated. The utility of the approach is explored for application as end-fired ultrafast optical amplifiers based on poly(9,9'-dioctylfluorene-co-benzothiadiazole). An internal gain of 19 dB was achieved on a 760 μm long waveguide at 565 nm wavelength. This fabrication procedure may be applied to a wide range of conjugated polymers and organic light-emitting devices, providing an important step towards future applications of organic integrated photonics.

©2009 Optical Society of America

OCIS codes: (130.5460) Polymer waveguides; (130.3130) Integrated optics materials; (140.4480) Optical amplifiers; (220.0220) Optical design and fabrication.

References and links

1. I. D. W. Samuel, and G. A. Turnbull, "Organic semiconductor lasers," *Chem. Rev. (Washington, D.C.)* **107**, 1272–1295 (2007).
2. D. Amarasinghe, A. Ruseckas, A. E. Vasdekis, G. A. Turnbull, and I. D. W. Samuel, "Amplification of optical pulse sequences at a high repetition rate in a polymer slab waveguide," *Appl. Phys. Lett.* **91**, 011105 (2007) and *Appl. Phys. Lett.* **92**, 149902 (2008).
3. D. Nilsson, S. Balslev, M. M. Gregersen, and A. Kristensen, "Microfabricated solid-state dye lasers based on a photodefinable polymer," *Appl. Opt.* **44**(23), 4965–4971 (2005).
4. M. Punke, S. Mozer, M. Stroisch, M. P. Heinrich, U. Lemmer, P. Henzi, and D. G. Rabus, "Coupling of organic semiconductor amplified spontaneous emission into polymeric single-mode waveguides patterned by deep-UV irradiation," *IEEE Photon. Technol. Lett.* **19**(1), 61–63 (2007).
5. M. Muccini, "A bright future for organic field-effect transistors," *Nat. Mater.* **5**(8), 605–613 (2006).
6. J. Yang, M. B. J. Diemeer, D. Geskus, G. Sengo, M. Pollnau, and A. Driessen, "Neodymium-complex-doped photodefined polymer channel waveguide amplifiers," *Opt. Lett.* **34**(4), 473–475 (2009).
7. G. Heliotis, D. D. C. Bradley, M. Goossens, S. Richardson, G. A. Turnbull, and I. D. W. Samuel, "Operating characteristics of a traveling-wave semiconducting polymer optical amplifier," *Appl. Phys. Lett.* **85**(25), 6122–6124 (2004).
8. R. Xia, G. Heliotis, Y. B. Hou, and D. D. C. Bradley, "Fluorene-based conjugated polymer optical gain media," *Org. Electron.* **4**(2-3), 165–177 (2003).
9. M. A. Reilly, B. Coleman, E. Y. B. Pun, R. V. Penty, I. H. White, M. Ramon, R. Xia, and D. D. C. Bradley, "Optical gain at 650 nm from a polymer waveguide with dye-doped cladding," *Appl. Phys. Lett.* **87**(23), 231116 (2005).
10. J. Clark, L. Bazzana, D. D. Bradley, J. Cabanillas-Gonzalez, G. Lanzani, D. G. Lidzey, J. Morgado, A. Nocivelli, W. C. Tsoi, T. Virgili, and R. Xia, "Blue polymer optical fiber amplifiers based on conjugated fluorene oligomers," *J. Nanophoton* **2**(1), 023504 (2008).
11. T. L. Koch, L. C. Chiu, and A. Yariv, "Analysis and performance of a picosecond dye laser amplifier chain," *J. Appl. Phys.* **53**(9), 6047–6059 (1982).

1. Introduction

Semiconducting conjugated polymers, due to their high optical gain and wide wavelength tunability, have been regarded as attractive materials for lasers, optical amplifiers and modulators, with the future potential to be electrically pumped [1]. The materials can be simply processed from solution to form low-loss waveguides, but one current limitation is that it is difficult to form well defined edge facets. The spin-coating process leads to poor quality edges, and the typically 100 nm thick polymer films do not cleave well to form facets [Fig. 1(d)]. As a result, lasers and optical amplifiers made from conjugated polymers have

usually been configured in surface-emitting geometries, using vertical microcavities or grating coupled configurations [1,2]. Edge-coupled conjugated polymer waveguides would be attractive for many applications, allowing for example the integration of polymer lasers to planar lightwave circuits for sensing and lab-on-a-chip [3,4]. End-fired optical amplifiers would avoid the use of grating couplers, which suffer from narrow bandwidth and potentially limit applications with ultra-short pulses. High quality optical facets would enable new applications such as edge emission from light-emitting field effect transistors (LEFETs) [5].

One possible approach could be to blend the active material with UV curable polymers and use photopatterning to define edge facets, as has previously been explored using dilute laser dyes [3,6]. However directly mixing conjugated and UV-curable polymers is unattractive because phase separation in polymer blends leads to high scattering loss. In this paper, we report an alternative approach to fabricate high edge-quality conjugated polymer waveguides, by encapsulating the conjugated polymer in a more brittle photo-crosslinked polymer that can readily be cleaved. To show the utility of the approach, we demonstrate them in high gain optical amplifiers.

2. Amplifier fabrication

To allow comparison with grating coupled optical amplifiers, we chose to use the conjugated polymer poly(9,9'-dioctylfluorene-co-benzothiadiazole) (F8BT) (from American Dye Source). The optical amplification of F8BT has previously been studied in both solution and grating coupled waveguide amplifiers [2,7]. For the edge-coupled amplifiers, a three-layered ridge configuration is used. The F8BT layer is sandwiched between layers of the negative photoresist SU8. In order to allow cleaving of edges for end-fired coupling, Si with 2 μm SiO₂ on top was used as substrate. Onto this a 460 nm SU8 film was first deposited by spin coating and cured with UV lamp. F8BT was then spin coated from 20mg/ml solution in toluene on the SU8 to form a 185 nm thick F8BT core layer. Next, a second layer of SU8 (420 nm thick) was deposited on top of the F8BT layer. The waveguide patterns were transferred to the top SU8 layer by standard photolithography. After the SU8 waveguides were developed, we used an extra washing step in toluene to remove the exposed F8BT layer. Figure 1(a) shows the

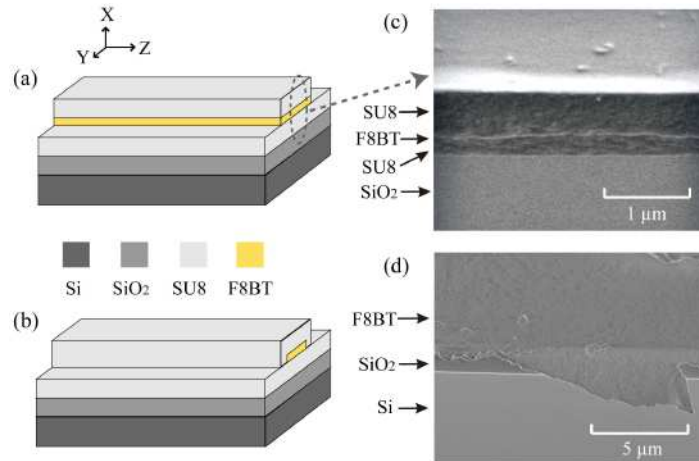


Fig. 1. (a), (b) diagrams of the finished sample in ridge and completely encapsulated configuration, respectively. (c) Electron micrograph showing the top surface and cleaved edge of a rib waveguide. The arrows indicate the composition of waveguide. (d) Electron micrograph showing the top surface and cleaved edge of an F8BT/ SiO₂/Si waveguide, showing the typical ragged edge of the conjugated polymer film. The images (c) and (d) are recorded from a 45 degree angle above the samples.

schematic of a finished sample. In some samples, a third layer of SU8 was overlaid on top of the previously defined waveguides and then patterned as a wider stripe, to achieve complete encapsulation of the SU8 core. The schematic of the finished samples is given in Fig. 1(b).

Finally, end facets were attained by cleaving the samples. To achieve high quality facets, a mark was first made on the top surface of the sample using a diamond scribe. The sample was then placed, with the waveguide facing up, on an aluminum platform, located above a sharp blade. The platform is configured such that when pressed down, the blade passes through a slot to make contact with the back face of the silicon. After the scribed mark was aligned with the hidden blade, the sample was pressed down gently with even force on both sides of the mark. A clean cleave propagates from the mark along the crystal axis of the Si and through the overlying polymer layers. Cleaved samples of 1 mm length with two clean edges were routinely achievable. The edge cross section of a 760 μm long waveguide, recorded by SEM, is displayed in Fig. 1(c).

3. Experimental characterization of the amplifiers, results and discussions

A potential concern with the processing is that the thermal cycling and UV curing may damage the light emitting properties of the semiconducting polymer layer. To estimate the impact of the processing, the steady state photoluminescence (PL) spectra and PL quantum yield (PLQY) of the sandwiched F8BT film were measured and compared with those of a pristine unprocessed F8BT film, each deposited on glass substrates. The excitation wavelength for both measurements was 442 nm. A PLQY value of 31% was obtained for the processed structure, compared to the value of 52% measured for the unprocessed F8BT film. The shape of the PL spectrum (shown in Fig. 2) was not affected by processing.

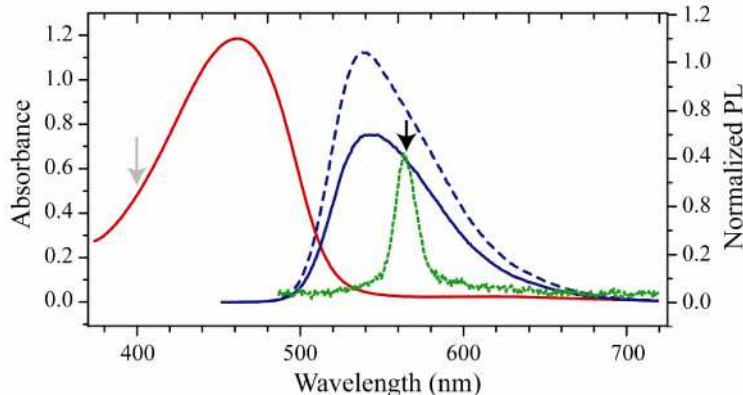


Fig. 2. Absorption (red solid line) and steady-state PL (dashed blue line) spectra of a pristine F8BT film spin-coated on SU8. The solid blue line shows the PL spectrum of the processed SU8/F8BT/SU8/glass structure. The dotted green line shows the ASE spectrum, measured using a ridge sample, configured as in Fig. 1(a). The arrows indicate the pump and probe wavelengths in the ultrafast amplification experiment.

To quantify the optical gain in the waveguide, the amplified spontaneous emission (ASE) threshold was measured for F8BT waveguides in both configurations [Fig. 1(a) and 1(b)] using a pulsed optical parametric oscillator (20 Hz, pulse width 4 ns) at an excitation wavelength of 442 nm. A typical ASE spectrum is given in Fig. 2. The intensities of the edge emission as a function of the pump energy density are plotted in Fig. 3(a). ASE thresholds, of 0.55 and 0.49 mJ/cm^2 for two waveguides [Fig. 1(a) and 1(b), respectively], can be easily extracted from the figure. These values are lower than that of an unprocessed F8BT film on SU8, 0.85 mJ/cm^2 , despite the reduced PLQY, suggesting that the ridge waveguide configuration enhances amplification of light traveling along the waveguide direction. The loss coefficient (α) of the waveguides at the ASE wavelength was determined by recording the change in ASE intensity as the pump beam is moved away from the end of the waveguides, as shown in Fig. 3(b). By fitting to an exponential attenuation function, we

obtained loss coefficients of 11.5 and 13.5 cm^{-1} for waveguides configured as in Fig. 1(a) and 1(b) respectively. These values are slightly higher than the 6.5 cm^{-1} loss of the unpatterned F8BT film on SU8 and 7.6 cm^{-1} loss for F8BT on SiO_2 [8], suggesting that, while the SU8 has low absorption, the ridge waveguide structure introduces a small additional scattering loss.

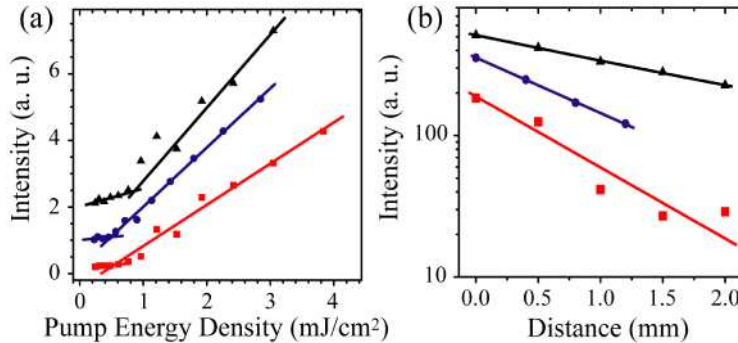


Fig. 3. ASE characteristics of three F8BT waveguides. Red squares are for a waveguide configured as Fig. 1(a), blue circles for a waveguide configured as Fig. 1(b), black triangles are for an unpatterned F8BT film on SU8. (a) Edge emission intensity as a function of pump energy density. (b) Dependence of ASE intensity on the distance between the pump beam and waveguide edge. Both data sets are offset for clarity.

Optical coupling and amplification in these waveguides was then characterized using a time-resolved pump-probe technique. A schematic of the experimental setup is given in Fig. 4. An optical parametric amplifier pumped by an amplified Ti-Sapphire laser system was used to generate pump pulses at 400 nm and probe pulses at 565 nm. All pulses were about 100 fs long (FWHM). The pump pulse was focused onto the top surface of the waveguide and the probe beam was coupled into the waveguides through a long working distance objective ($\times 20$). The output light was collected by another objective ($\times 8$) and then focused to a spectrally and time-resolved streak camera. All experiments were carried out in air. To calculate the input coupling efficiency, the transmission of the probe light through the waveguide was measured (with the pump off). The power coupled into the waveguide at the input edge was then estimated using the previously measured loss coefficient α , and assuming a 100% output coupling efficiency. An input coupling efficiency of 11% was achieved on the waveguides.

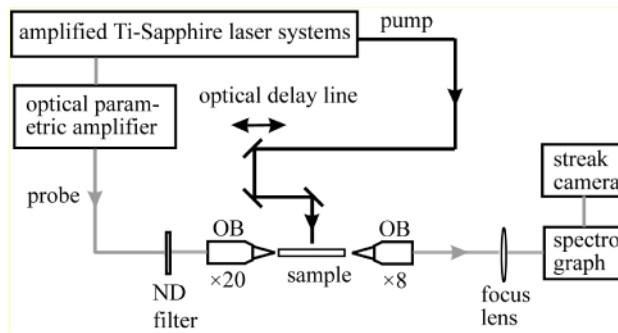


Fig. 4. Schematic of the time-resolved pump-probe experimental setup. OB=objective, ND=neutral density. The pump path is indicated by black lines, and the probe and total signal path by light grey lines.

Figure 5(a) shows three typical time traces of the output from the waveguide: the probe signal with no pump applied, the amplified output signal and the PL background measured at the same excitation energy density but without the probe pulse. The width of the output pulse

is limited by the response function of the streak camera, which is about 3 ps at FWHM. The amplified signal is extracted by subtracting the PL background from the total output signal, as shown in typical streak camera measurements in Fig. 5(b). The internal optical gain was calculated using the equation

$$G(\text{dB}) = 10 \log\left(\frac{P_{on} - P_{PL}}{P_{off}}\right) = 10 \log(G) \quad (1)$$

where P_{on} is the total output signal, P_{PL} is the PL background, and P_{off} is the probe signal in the absence of pumping. From Fig. 5(a) and 5(b), a gain of 13 dB is obtained for a 760 μm long ($1.1 \mu\text{m} \times 200 \mu\text{m}$ cross section) waveguide [Fig. 1(a), 1(c)], when probed with 29 pJ input signal and pumped with energy density of $63 \mu\text{J}/\text{cm}^2$.

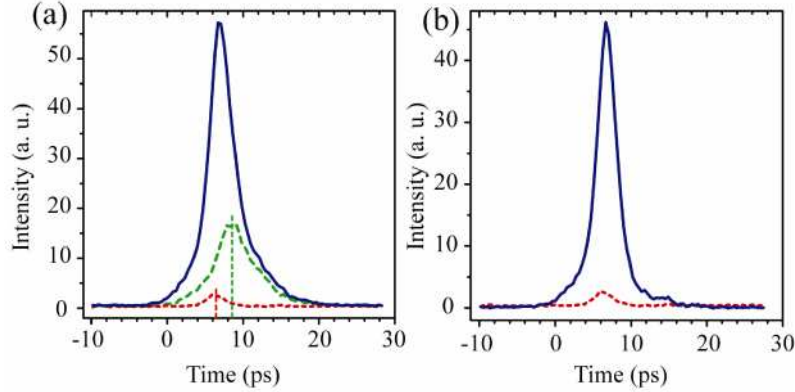


Fig. 5. (a) Typical time traces of the probe signal (dotted red) only, PL background (dashed green), and the total amplified output (solid blue) from a 760 μm long sample as in Fig. 1(a). (b) Corresponding amplified probe signal (with PL background subtracted from the total output) and probe signal.

Gain as a function of pump energy density is plotted in Fig. 6(a). The gain increases with increasing pump energy density up to around $60 \mu\text{J}/\text{cm}^2$. The saturation of gain at higher pump energy may be explained by exciton annihilation and competition with ASE. The maximum internal gain of 19 dB is observed for the input pulse of 8 pJ, and corresponds to a net external gain of 6 dB. The internal gain is equivalent to 250 dB/cm, significantly higher than the 9.3 dB/cm and 0.35 dB/cm, reported previously for doped PMMA waveguides [9,10]. The product of gain cross section σ and exciton density N of the waveguide can be derived from the linear range of the gain curve using $G = f\sigma NL$, where f is the fractional overlap of the waveguided probe light with the excitation profile of the F8BT film and $L=0.76 \text{ mm}$ is the length of the pumped waveguide. The fitting yields $f\sigma N = 58 \text{ cm}^{-1}$ at a pump energy density of $63 \mu\text{J}/\text{cm}^2$. This pump density corresponds to $N = 5 \times 10^{18} \text{ cm}^{-3}$ in the active 185 nm F8BT layer, where 80% of pump energy is absorbed. Using these numbers and assuming $f \approx 0.25$ we get $\sigma \approx 5 \times 10^{-17} \text{ cm}^2$, in good agreement with the previously reported value for F8BT optical amplifiers [2].

The variation of gain with the probe signal energy was also studied on the same waveguide, as shown in Fig. 6(b). As expected, we observe that gain decreases with the increase of probe energy, due to gain depletion. While the ridge waveguide strongly confines the probe light perpendicular to the film, the 1.4 μm diameter input beam expands in the plane of the 200 μm wide ridge as it propagates. To model the effect of gain saturation we therefore need to account for this expansion in the well-know net gain equation for pulsed pump-probe system [11]. We divide the waveguide into 100 portions and calculate the accumulated gain of each portion using the net gain equation. The total gain is the product of gains corresponding to each small portion:

$$G = \prod_{n=1}^{100} \frac{1}{S_n} \ln [1 + g_0 (\exp(s_n) - 1)] \quad (2)$$

where $S_n = E_{in}^n (\sigma_{abs} + \sigma_{se}) / A_n h \nu_{in}$, E_{in}^n is the probe input energy at the n th section, which is the output energy from the $(n-1)$ th section, G_0 is the unsaturated gain, σ_{abs} and σ_{se} are the absorption and stimulation emission cross section, respectively, A_n is the cross sectional area of the probe beam at each small portion, and ν_{in} is the frequency of the probe signal. $A_n = 2w_0 t (1 + (2z_n / kw_0^2)^2)^{1/2}$, where w_0 is half of the width (in y direction) of the probe beam at the entrance face ($0.7 \mu\text{m}$) and t is the thickness of the F8BT film. Fitting to the modified net gain Eq. (2) yields total unsaturated gain G_0 of 22 dB.

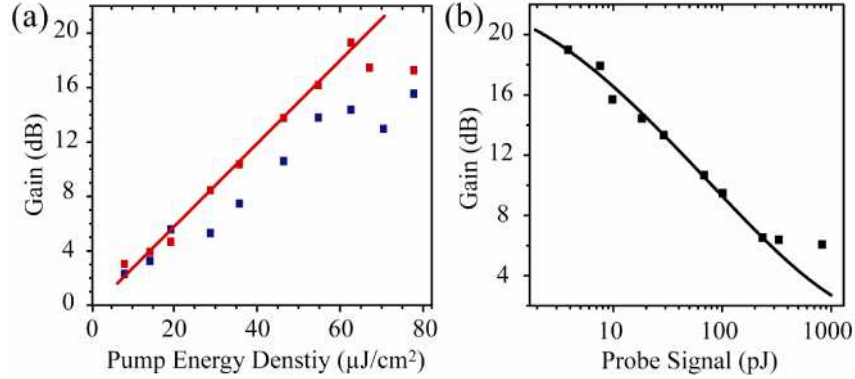


Fig. 6. (a) Gain as a function of pump energy density. Data indicated by red squares are obtained from probe energy 8 pJ, blue squares are from probe energy 29 pJ. (b) Gain as a function of probe signal energy at pump energy density $63 \mu\text{J}/\text{cm}^2$. Black curve is the theoretical fit to Eq. (2).

We note that the end-fired amplifier requires higher pumping energy density, compared to the previously reported grating-coupled F8BT amplifiers, which used a polymer film spin-coated on a fused silica substrate [2]. This could be explained by a reduced confinement factor (by 3.5 times to $\sim 20\%$) of the waveguided probe beam in the gain medium in the present work. Simple optical mode calculations reveals three possible TE modes in the sandwiched F8BT waveguide structure. However, only the TE_0 mode shows a good overlap with the gain medium. Even though the TE_1 mode is difficult to couple into the structure for symmetry reasons, the TE_2 mode can be easily coupled into the waveguide with much of the mode confined in the SU8 layers. This may explain the need for higher pump energies for comparable gain in the current waveguides. Further increasing the thickness of the middle F8BT layer, and reshaping the probe beam profile should further improve the optical mode overlap with the gain medium and the coupling, and therefore the performance of the end-coupled amplifiers.

4. Conclusion

In summary, we demonstrated an improved method to fabricate conjugated polymer waveguides with well-defined facets. This new fabrication procedure may be applied to a wide range of conjugated polymers, given that the thermal cycling during fabrication does not alter the optical properties of the material considerably. These waveguides could show great potential in future broadband ultra-short optical pulse applications. Edge-emitting lasers, optical amplifiers and switches, and LEFETs may also find wider applications in integrated optical circuits than their surface emitting counterparts.

Acknowledgments

We are grateful to EPSRC for financial support, including the HYPIX project, and to W. Whelan-Curtin and T.F. Krauss for assistance in taking SEM images.